NEW DIRECT ACTING ANTI-VIRALS INHIBITING HEPATITIS C VIRUS HELICASE AND INSIGHTS INTO HOW ATP FUELS HELICASE ACTION

by

Mark Yerukhimovich

A Thesis Submitted in

Partial Fulfillment of the

Requirements for the Degree of

Master of Science

in Chemistry

At University of Wisconsin-Milwaukee

May 2018

ABSTRACT

NEW DIRECT ACTING ANTI-VIRALS INHIBITING HEPATITIS C VIRUS HELICASE AND INSIGHTS INTO HOW ATP FUELS HELICASE ACTION

By

Mark Yerukhimovich

The University of Wisconsin-Milwaukee, 2018
Under the Supervision of Professor David N. Frick

According to the World Health Organization, Hepatitis C Virus (HCV) has infected 130-150 million people worldwide. Approximately 700,000 of those die each year from chronic HCV related causes such as cirrhosis or cancer. Currently, there are numerous HCV drugs on the market; they target the protease, polymerase and NS5A proteins encoded by of HCV. These drugs are expensive and HCV can become resistant, thus there is constant need for new DAAs. The first part of this thesis examines the search for additional drugs that function by inhibiting the NS3 helicase, which have been challenging to develop.

Part of the reason for a lack of helicase inhibitors can be due to the difficulty of understanding its mechanism. The helicase is a motor protein that couples ATP hydrolysis to DNA or RNA unwinding. The second part of this thesis examine the role of a cysteine residue in the helicase ATP binding site. When the cysteine was replaced with other amino acids, the protein possessed unusual features not seen in the wildtype helicase. Helicase proteins lacking the cysteine, were able to hydrolyze ATP in the absence of nucleic acid 15times faster than wildtype. This finding may provide future information into the coupling mechanism of chemical energy to physical motions of the enzyme.

TABLE OF CONTENTS

LIST OF FIGURES v

LIST OF TABLES vi

LIST OF ABBREVIATIONS vii

ACKNOWLEDGMENTS viii

Chapter 1: Literature Review 1

Section 1.1: Background 1

Section 1.2: NS3 Protease Drugs -previr 2

Section 1.3: NS5B Polymerase Drugs -buvir 7

Section 1.4: NS5A Phosphoprotein Drugs -tasvir 10

Section 1.5: Summary 12

Section 1.6: NS3 helicase Drugs 13

Chapter 2: Methods 14

Section 2.1: Site Directed Mutagenesis and Protein Expression 14

Section 2.2: Colorimetric ATP Hydrolysis Assays 15

Section 2.3: Continuous coupled ATP Hydrolysis Assay 15

Section 2.4: DNA Binding Assay 15

Section 2.5: Helicase Unwinding Assay 16

Section 2.6: Intrinsic Protein Fluorescence 16

Chapter 3: Screening for DAAs targeting HCV helicase 18

Section 3.1: Novel Pyrrolone Inhibitors 18

Section 3.2: Novel Piperazine Inhibitors **19**

Section 3.3: Novel Thieno-pyrimidine Inhibitors **19**

Section 3.4: Novel symmetrical phenylenediamine Inhibitors **20**

Section 3.5: Novel Bicyclic octahydrocyclohepta[b]pyrrol-4(1H) one Inhibitors **20**

Chapter 4: Role of Cys292 in Coupling RNA binding to Helicase-catalyzed ATP Hydrolysis **21**

Section 4.1: Background **21**

Section 4.2: Results **22**

Section 4.3: Conclusions **24**

TABLES **26**

FIGURES **32**

BIBLIOGRAPHY **47**

LIST OF FIGURES

Figure 1: Structure of synthesized novel pyrrolone HCV NS3h inhibitor 7c. 32

Figure 2: Piperazine compounds and relevant *in vitro* screening results. 33

Figure 3: Structure of Thieno-pyrimidine compound 1a. 34

Figure 4: Intrinsic Protein Fluorescence for Determination of K_d. 35

Figure 5: Positions of Cysteines in of HCV helicase. 36

Figure 6: Structures of open and closed HCV helicase conformations 37

Figure 7: Random Sequential Mechanism of ATP and RNA binding to HCV helicase. 38

Figure 8: DNA Sequencing results showing the desired mutation encoding C292G. 39

Figure 9: Helicase unwinding assays with the wildtype and C292G helicases 40

Figure 10: DNA binding assays to characterize dissociation constant for ssDNA 41

Figure 11: ATPase assay to approximate enzyme affinity for Poly-U RNA (K_{RNA}) 42

Figure 12: Stimulated ATPase to characterize specific activity in the presence of RNA. 43

Figure 13: Stimulated ATPase assay to estimate affinity for Mg*ATP. 44

Figure 14: Unstimulated ATPase to characterize the specific activity of both enzymes. 45

Figure 15: Unstimulated ATPase assay to estimate affinity for ATP. 46

LIST OF TABLES

Table 1: Pyrrolone compound screening results. 26

Table 2: Piperazine compound screening results. 27

Table 3: Selected Thieno-pyrimidines for helicase inhibition analysis. 28

Table 4: Thieno-pyrimidine Helicase unwinding assay results. 29

Table 5: Phenylenediamine derivatives and HCV genotype 1b inhibition. 30

Table 6: Octahydrocyclohepta[b]pyrrol-4(1H) one derivatives and cell based inhibition. 31

LIST OF ABBREVIATIONS

HCV: Hepatitis C Virus

NS3h: Nonstructural Protein 3 helicase

DAA: Direct Acting Antiviral

CYP3A4: Human cytochrome p450 isoform 3A4

MBHA: Molecular beacon helicase assay

IC_{50}: Inhibitor concentration at which activity is decreased 50%

CC_{50}: Cytotoxicity concentration. Concentration of inhibitor that reduces live cell count by 50%

SAR: Structure activity relationship

ACKNOWLEDGMENTS

I would like to thank my advising professor first and foremost, for the opportunity to come back to UWM to continue my undergraduate research and turn it into a graduate degree. Rotating in the Frick Lab gave me a true taste of scientific inquiry at the forefront of Biochemical research. I value the opportunity given to me to work on drug discovery and mechanistic studies. Dr. Frick has dedicated a lot of his time and wisdom to my work and I appreciate it and look forward to continuing the scientific quest ahead. This thesis and my success stem from his continued commitment to me and his students.

To my lab members, I wish you luck in your research and funding quests. You have a great adviser with you, as well as a very helpful faculty that is always open to collaboration.

Last, I would like to thank my wife and newborn son for their continued support and patience while I completed my degree. Amie, you deserve all the praise I have, for helping me by caring for our son, supporting me through difficult times, and giving me helpful reminders to write! To my immediate family, thank you for your continued support and the opportunity to grow up in the United States.

Chapter 1: Literature Review

Section 1.1: Background

Hepatitis C Virus (HCV) [1] chronically infects an estimated 70 million people worldwide. Of those, roughly four hundred thousand die each year from cirrhosis or liver cancer. According to the CDC, one quarter of people with HIV also are co-infected with HCV. This complicates for treatment of either disease and can increase risk for life-threatening complications. However, with modern advances in disease research, numerous direct acting antivirals (DAAs) have been created to effectively cure over 95% of all those living with HCV [2]. Current barriers to treatment are cost and the lack of symptoms for many, while infected.

HCV is an enveloped virus which is transmitted via blood-to-blood contact. It primarily infects the liver and can be asymptomatic for many years until it leads to liver disease. There is no vaccine currently on the market, however, with extensive research of the viral proteins, in 2011, the first class of DAAs was released and offered a cure to many. Prior treatment, with pegylated interferon and/or ribavirin, offered an increased chance for a person's body to fight off the infection, but had side effects and was an expensive treatment. The current treatments have few side effects, and with insurance, can be an affordable cure. A culmination of research in virology, biochemistry, and medicinal chemistry has provided relief for many.

HCV belongs to the *Flaviviridae* family of single-stranded, positive-sense RNA (+) ssRNA viruses. Upon infection, the virus enters the cell and releases its genetic content. The (+) ssRNA is like mRNA in eukaryotes; it does not need any modifications and is ready to be translated by host ribosomes. The viral RNA is translated into a single polyprotein that is cleaved into mature

proteins: structural (core, E1, and E2) and nonstructural (p7, NS2, NS3-4A, NS4B, NS5A, and NS5B). The core, E1, and E2 are integral to the formation of core and envelope glycoproteins for viral particle synthesis. NS2 and p7 support new viral particle formation, but are not incorporated into the mature virus. NS3:NS4A, NS4B, NS5A and NS5B form the replicase responsible for replicating the RNA viral genome. [3]

There are numerous HCV drugs on the market as well as many others in clinical trials. The drugs can be administered as a single drug, or a combination of drugs targeting one, or many HCV protein targets as well as genotypes. There are three main classes of HCV DAAs: NS3/4A serine protease inhibitors, NS5A protein inhibitors, and NS5B RNA polymerase inhibitors. I will discuss the current advances in each class.

Section 1.2: NS3 Protease Drugs -previr

NS3 is a multifunctional protein complexed with its cofactor, NS4A. NS3 is composed of a serine protease in its N terminus, vital to polyprotein processing and viral replication, and a NTPase/RNA helicase in its C-terminus. The NS4A cofactor is located at the C terminus of NS3. [4]. NS4A is a short 54 a.a. peptide that is required for correct NS3 folding and NS3/4A membrane tethering. Both the NS3 helicase and protease have been studied extensively, and numerous crystal structures have been solved.

NS3 protease is a serine protease with a chymotrypsin-like fold, composed of 2 beta barrels flanked by two alpha helices. The active site of the protease can accept between 6 and 10 amino acids; efficiency of the enzyme is best with ten. The NS4A cofactor helps position the substrate into the active site and contributes to substrate specificity. General substrate notation are the ten amino acid positions; P_6 through $P_{4'}$. The $P_1 – P_{1'}$ peptide bond is the one

cleaved; the scissile bond. The active site catalytic triad is composed of: His 57, Asp 81, and Ser 139. Lemke and associates demonstrate non-catalytic residues that are important to substrate binding and in important for inhibitor design [5]. R155 and D168 form a salt bridge when substrate is bound. The salt bridge induces the aliphatic chains of the residues to be exposed forming a hydrophobic pocket in the active site. The general mechanism of the protease is well known.

First, the substrate binds and is positioned correctly in the active site. The histidine deprotonates the serine hydroxyl group thus activating to attack the carbonyl carbon of the substrate. This create a tetrahedral intermediate. The amide bond is broken and electrons are transferred to the histidine. This breaks the scissile bond and regenerates the histidine, while the serine is still bound to the carbonyl carbon of the substrate. The N terminus of the substrate exits, and a water enters that is activated by the histidine. The activated water attacks the carbonyl carbon of the substrate forming another tetrahedral intermediate. A subsequent electron transfer, kicks off the serine and regenerates both the His and Ser residues. The carboxy-terminus of the substrate can now leave the active site. The aspartic acid residue acts as a hydrogen bond acceptor from the delta amine of histidine. This subsequently pulls the electrons from the epsilon nitrogen making it a better electrophile for attack on the serine hydroxyl group. N-terminal peptides will serve as an important starting point for the development of NS3 protease inhibitors [6].

Landro J. A. and associates showed that NS3 protease catalytic rate is substrate sequence specific and amplified by about 5 times in the presence of cofactor NS4A [7]. NS3 protease is responsible for cleaving the translated initial polyprotein at: NS3/NS4A, NS4A/NS4B,

NS4B/NS5A, and NS5A/NS5B junctions for the activation of those proteins for viral replication and particle formation. Research has cataloged the amino acid residue sequences as well as *in vitro* catalytic rates; the cleavage of NS5A/NS5B is more efficient than other sites. The amino acids essential for activity are an acidic residue in P6, a cysteine in P1, serine or alanine in P1' and a hydrophobic residue in P4'. Steinkühler et al. showed that as substrate concentration (DEMEEC-ASHLPYK-NH_2 of the NS4A/NS4B site) was increased in steady state analysis, the apparent K_m increased as well, while no change observed for k_{cat} [8]. Thus, the first example of competitive product inhibition was discovered. The researchers aimed to confirm this was a true observation and developed the N and C terminus polypeptides (DEMEEC-OH, ASHLPYIEQG) and found that the N terminus substrate (DEMEEC-OH) competitively inhibited NS3 protease with a K_i of 600 nM. They tested the substrates for the other junctions as well. Both the NS4A/NS4B and NS5A/NS5B had K_m values sub 10 µM and the N terminus peptides had K_i values in the micromolar range. To note, there was no inhibition up to 500 µM substrate, with the NS3/NS4A substrate. This show NS3 protease cleaves the NS3/NS4A junction and there is no product inhibition. This evidence shows a possible target for drug development, as inhibition at this junction could impede further polyprotein cleavage and thus halting viral proliferation.

The DEMEEC-OH peptide was further studied and optimized by Ingallinella et al. This group optimized each possible position of P6-P1 to create the hexamer Ac-Aspartate-Glutamate-3,3-diphenylalanine-Glutamate-β-cyclohexaylalanine-Cysteine-OH (Ac-Asp-Glu-Dif-Glu-Cha-Cys-OH) [9]. This peptide substrate had a K_i of 50 nM and was a fundamental contribution to the discovery of the first class of NS3 protease inhibitors; reversible covalent

ketoamide binders boceprevir and telaprevir. Another class of inhibitors discovered were reversible non-covalent ketoamide macrocycles.

The macrocycles are the current class of protease inhibitors on the market. The first generation had three breakthrough drugs: Ciluprevir, BMS-605339, and MK-4519. Ciluprevir was a P1-P3 macrocycle. It never reached the market due to safety issues in clinical trials. The *in vitro* studies provided evidence of a potent inhibitor and important moieties that would lead to improvements of further drugs. Llinas-Brunet and associates showed that a P1 vinylcyclopropylcaboxylic acid moiety that yields good solubility, good potency, and selectivity. Ciluprevir also added to selectivity by making extra hydrogen bonds in the active site and adding structural rigidity of the extended peptide [10].

Another key discovery was BMS605339 [11]. This was an acyclic molecule and instead of a vinylcyclopropylcaboxylic acid at P1. Scola and team performed a structure activity relationship, SAR, on a parent hexapeptide and determined a cycloproplacylsulfonamide in the P1 position was best corresponding to a 50-fold decrease in IC_{50} (to 1 nM) than the carboxylic acid. The sulfonamide moiety provides additional interactions with Gly137 and Ser139 in the active site as well as maintains and ionic interaction with His57. While BMS605339 did not pass clinical trials due to cytotoxicity, it provided the elucidation of the sulfonamide moiety.

Last, Liverton and associates showed that molecular docking of the inhibitors above, revealed inhibitor P2 positions in an empty part of the protease crystal structure [12]. The researchers determined that the empty electron density around the P2 position was missing the NS3 helicase interaction. This is a valid consideration knowing that *in vivo* the NS3 is a multifunctional protein. MK-4519 was determined through a structure activity relationship,

SAR, study by modeling and performing inhibitor studies *in vitro* with genotype 1b full length NS3/4A. The vinylsulfonamide, from BMS-605339 was retained, the similar isoquinoline moiety of ciluprevir and BMS-605339 in the P2' position was simplified and MK-4519 was developed. MK-4519 has a K_i sub nanomolar and an IC_{50} of about 5 nM. This compound is 50,000-fold more selective to NS3 than tryspin or chymotrypsin; similar active site, proteases. While these three compounds laid the ground work for future protease drugs, they had a few weaknesses: they were susceptible to NS3 resistance mutations, they were expensive therapies, and they were only effective on genotype 1b.

The current generation of macrocycles can cure HCV patients with most of the genotypes without the need for interferon when combined, with a NS5A inhibitor, NS5B inhibitor, or both. I will focus on two current protease inhibitors paritaprevir [13] and grazoprevir [14]. Paritaprevir was developed by Abbott in 2010 and is a component of VIEKERA PAK. It is a P1-P3 macrocycle with a acylsulfonamide, a P4 methyl pyrazine, and a phenanthridine moiety at P2. The P4 and P2 moieties interact with D168 and R155 respectively. These are common genotype 1 residues that can be mutated and confer resistance to inhibitors. Paritaprevir is designed off the discoveries of previous protease inhibitors such as faldaprevir by Boeringer Ingelheim [15]. D168 and R155 are common locations of mutations, and O'meara and team discovered that reducing the interactions at those sites make the inhibitor less sensitive to resistance. The P4 and P2 moieties are designed then to interact via hydrophobic interactions rather than more specific interactions like hydrogen bonds or salt bridges. Paritaprevir has *in vitro* IC_{50} in the low nanomolar range and is affective against genotypes 1a, 1b, 2a, 3a, 4a, and 6a, however, with reduced sensitivity to genotype 3a due to a D168Q mutation. Paritaprevir, as

mentioned above, is a component of Viekera PAK. The other components are ombitasvir, ritonavir and dasabuvir. The combined therapy is a new approach to target all stages of viral replication; ombitasvir targets the NS5A multifunctional protein, dasabuvir targets the NS5B RNA polymerase, and ritonavir (anti-HIV) targets cytochrome P450 to reduce the metabolism of paritaprevir in the plasma. Viekera PAK can cure genotype 1a and 1b in 12 weeks and costs between $80,000-$170,000, depending on duration of treatment required.

Grazoprevir was developed in 2012 by the Harper team at Merck [14]. It is a component of Zepatier and while approved as a genotype 1 and genotype 4 cure, it is a potent inhibitor for genotypes 1-6. Grazoprevir is a P2-P4 macrocycle containing an N terminal acylsulfonamide, a P2 aromatic quinoxaline which decreases aqueous solubility causing the drug to have elevated levels in the liver, and a P4 cyclopropyl group which allows space for A156 mutants. Grazoprevir is an important drug molecule as it is a tight binder, low or sub-nanomolar concentrations, to common genotype 1 mutants R155K, A156T, A156V, and D168V. Grazoprevir is combined with elbasvir, a NS5A inhibitor. Zepatier can cure HCV genotype 1 and 4 in 12-16 weeks and is a remarkably cheaper option starting at around $50,000 for 12 weeks.

Section 1.3: NS5B Polymerase Drugs -buvir

The NS3 protease inhibitors were the first HCV drugs on the market; NS5B polymerase inhibitors followed shortly after. NS5B is a RNA polymerase necessary for viral RNA replication but is error prone due to lacking proofreading mechanism. It is composed of 591 amino acid and is homologous to other RNA dependent polymerases. It has 6 motifs, A-F, with the key motif “GDD” located in the N-terminus and is membrane tethered by 21 amino acids in the C-terminus. The general shape of the polymerase is that of a right hand containing a finger, palm

and thumb domain. NS5B has an encircled active site with numerous interactions between the finger and thumb domains and uses two catalytic magnesium ions. The thumb domain contains a β-hairpin loop, which influences the positioning of newly synthesized RNA, and can also modulate the different modes of replication; either *de novo* without primer and create its own dinucleotide to serve as a single stranded primer (closed polymerase) [16], or primer dependent, transcribing from the 3' end of a double stranded RNA molecule (open polymerase) [17]. The two different modes of replication are remarkably different. The *de novo* process has two slow steps followed by the rapid processivity of the polymerase. The two steps require the synthesis of dinucleotide primer, followed by, the use of the newly synthesized primer. The next nucleotide needs to be present in high concentration for elongation to occur. The presence of high concentration of GTP stimulates the switch of synthesis to elongation [18].

There are two types of polymerase inhibitors available currently on the market on in trials: nucleotide analogs, and non-nucleotide inhibitors. Nucleotide inhibitors are designed to target the polymerase active site by being incorporated into the growing RNA strand but hindering further elongation due to steric hindrance at the 2' position on the ribose sugar. They can be competitive inhibitors with regards to substrate nucleotides. Non-nucleotide inhibitors are considered non-competitive as they do not compete with the substrate nucleotides, but rather, they bind the polymerase and effectively block conformational changes required for elongation steps [19]. The two drugs I will discuss are sofosbuvir, a nucleotide analog pro-drug, and dasabuvir, a palm domain-specific inhibitor.

Sofosbuvir was developed by Pharmasset, acquired by Gilead, by the Sofia team [20]. Under the nucleoside class, there are three sub classes, β-D-2'-deoxy-2'-α-F-2'-β-C-

methylribose, β-D-2’-β-methylribose, and 4’-azidoribose classes. Sofosbuvir is a β-D-2’-deoxy-2’-α-F-2’-β-C-methylribose prodrug that has a phosphoramidate moiety at the 5’ position on the sugar. It was developed so that the phosphoramidate moiety would be cleaved and quickly phosphorylated (30 minutes to 2 hours post-dose detection) to the active 2'-deoxy-2'-α-fluoro-β-C-methyluridine-5'-triphosphate in the liver. It is done so by hydrolyzing the carboxy ester by human Cathepsin A. Next an elimination of the phenol forms an alaninyl phosphate metabolite which is removed by histidine triad nucleotide-binding protein 1 to give the 2'-deoxy-2'-α-fluoro-β-C-methyluridine-5'-monophosphate. Last, the monophosphate is phosphorylated twice, first by UMP-CMP kinase, and then by nucleoside diphosphate kinase to give the active triphosphate product [21]. The Sofia group showed that the more active diastereomer PSI-7977 could generate 29 μM triphosphate when incubated in hepatocytes with no cytotoxicity. Once the active triphosphate is incorporated into the replicating RNA, the next nucleotide cannot be added due to steric hindrance at the 2’ position. The active phosphate has sub to low micromolar IC_{50} value *in vitro* inhibition for genotypes 1b, 2a, 3a, and 4a. The active triphosphate is also not a substrate for other eukaryotic polymerases nor mitochondrial RNA polymerase. *In vivo* studies by Lam and associates showed that the common mutation S282T showed reduced susceptibility to the active triphosphate in genotypes 1b. 2a. 3a. and 4a [22], however, still being able to cure HCV infection within 12 weeks. Sofosbuvir was approved by the FDA in 2013 and is still currently on the market as part of a cross-genotypic cure, Epclusa. Sovaldi, composed of only sofosbuvir, costs about $84,000 for a 12-week treatment and is approved for genotypes 1-4. Epclusa is priced a little lower at about $75,000 for a 12-week treatment.

The other type of polymerase inhibitor is a non-nucleotide inhibitor. Non-nucleotide inhibitors can target the various structural domains of the polymerase: thumb, finger, or palm, however, the lack of sequence conservation in these domains, the non-nucleotide inhibitors are usually single genotype specific. Non-nucleotide inhibitors target allosteric sites on the thumb: T1 and T2, the palm: P1 and P2, and the β-hairpin: P-β. Benzothiadiazine derivatives were shown to be potent inhibitors of that targeted the P1 site, however were susceptible to resistant variants. Dasabuvir was discovered by Liu and associates at Abbott [23]. It is an aryl dihydrouracil derivative that acts by binding the polymerase palm domain with low nanomolar IC_{50} for genotype 1a and 1b *in vitro* and also low nanomolar IC_{50} *in vivo*. Kati and team showed dasabuvir's specificity to HCV polymerase, not affecting various eukaryotic polymerases, as well as catalogued resistant variants [24]. Dasabuvir is a component of Viekira PAK. It contains the protease inhibitor paritaprevir, and the NS5A inhibitor ombitasvir. There is also ritonavir which is necessary to suppress the activity of human cytochrome p450 isoform 3A4 (CYP3A4) which will metabolize various inhibitors [25]. VIEKERA PAK can cure genotype 1a and 1b in 12 weeks and costs about $80,000 for a 12-week treatment.

Section 1.4: NS5A Phosphoprotein Drugs -tasvir

The last type of HCV DAAs available is the class of NS5A inhibitors. NS5A is a multifunctional, endoplasmic reticulum membrane associated, phosphoprotein. It is responsible for viral replication and viral assembly as shown by Shirota [26]. Arima and associates showed that NS5A can modulate hepatocyte growth by interacting with cyclin-dependent kinases; necessary for eukaryotic cell cycle proliferation and progression [27]. Ghosh and associates showed that in mice, NS5A caused uncontrolled growth of fibroblasts and tumor

formation [28]. Last, Lan and associates showed the NS5A directly binds tumor suppressor p53. By sequestering p53, apoptosis of HCV infected cells is decreased and therefore allows HCV proliferation; contributing to liver cancer in chronic infections [29].

NS5A is composed of 447 amino acids with 4 distinct regions: The N-terminal amphipathic helix, the serine rich phosphorylation cluster, the interferon sensing region responsible for inactivating protein kinase R (host protein responsible for mounting a response against viruses), and the proline rich cluster in the C-terminus [30]. The proline rich cluster is conserved throughout all HCV genotypes and thus is a good drug target. The N-terminal helix is required for functional NS5A and key mutations abolished HCV replication *in vivo* [31]. It is also characterized as a zinc binding protein that can interact with viral RNA for replication. It is non-enzymatic and has a diverse but not well-defined role in the HCV lifecycle. I will focus on two drugs, daclatasvir and velpatasvir, that have similar modes of inhibition and similar drug design.

Daclatasvir is a first generation NS5A inhibitor. It was developed by Bristol-Myers Squibb in 2013. It was designed on SAR based off a symmetric NS5A inhibitor from Bristol-Myers Squibb in 2009 [32]. This work provided the scaffold of a symmetric compound, that had resistance to mutations in Domain I of NS5A; Y93H, L31V, and Q54L. The 2009 work also showed that these NS5A compounds also inhibited hyperphosphorylation. Daclatasvir has IC_{50} values in the low picomolar range *in vivo* for genotypes 1a and 1b, sub-nanomolar IC_{50} for genotypes 2-5, and is specific to HCV. Daclatasvir was also shown to interact only with domain 1 of NS5A and not with NS3 or NS5B. Ascher and associates show that daclatasvir competes with RNA binding and by *in silico* docking showed the possible interactions at the dimer interface of domain 1 [33]. Daclatasvir has a biphenyl core with symmetrical branched elements. Guedj and

team demonstrated daclatasvir is a potent inhibitor as it can block both RNA synthesis and virus assembly [34]. Daclatasvir is marketed as Daklinza and was approved in 2015 to be used with sofosbuvir to treat genotype 3 patients without interferon or ribavirin. The cost is about $150,000 for a 12-week combined therapy.

Velpatasvir, a component of Epclusa, can treat HCV genotypes 1 through 6. It was developed by Gilead in 2013 and was approved as a combination therapy with sofosbuvir in 2016. It has *in vitro* HCV inhibition at picomolar concentrations [35]. It binds in domain 1 and is a defective substrate that competes with RNA. It is not symmetrical and thus the structure of it makes it less sensitive to domain 1 common mutations than is daclatasvir. Both drugs contain an imidazole proline component, however, velpatasvir also contains a benzopyrano imidazole core which itself is not symmetric. Lawitz and associates showed that velpatasvir has better *in vitro* activity against genotype 2 and 3 than daclatasvir [36]. Velpatasvir is also effective against genotypes 1a, 1b, 2, 3, and 4 in patients mimicking the *in vitro* results of Cheng. Currently Epclusa cost $75,000, and is a once a day pill for 12 weeks that cures HCV infection.

Section 1.5: Summary

The drugs covered above have shown the combined work of biochemistry, virology, and medicinal chemistry. Combination therapies can target more genotypes and are also able to be less sensitive to common resistant mutations. Here are a few current therapies that were approved this year: Vosevi from Gilead (sofosbuvir/velpatasvir/voxilaprevir), MAVYRET from Abbvie (glecaprevir/pibrentasvir). Both are pangenotypic and cheaper than EPCLUSA. HCV drug development is continuing and new drugs are in clinical trials from Merck and Janssen [37]. HCV therapies need to be developed as resistant mutations are discovered. The one protein not

mentioned in current therapies is the HCV NS3 helicase. NS3 helicase is a viable drug target as it a necessary component to the HCV lifecycle and there are no current drugs that target NS3 helicase on the market.

Section 1.6: NS3 helicase Drugs

Various *in silico* studies have identified possible inhibitor scaffolds by utilizing molecular docking programs like DOCK or ROCS. Once general properties of protein sites are identified, drug molecules can be optimized. Another drug identification technique is to screen readily available drug compound libraries *in vitro* or *in vivo* to identify a hit and further perform SAR to optimize the inhibition of the compound. Chen *et al.* showed how the use of DOCK as a virtual screening method of known compounds [40]. This study lead to the crystal structure of NS3h with a blue HT dye bound in between domains 1 and 2. An earlier study by an Italian group, identified a nucleotide mimicking inhibitor that was designed off a known HIV reverse transcriptase selective molecule [41]. The two studies above helped guide further studies that developed possible drug leads by using *in silico* screening of molecule design [42-45]. High throughput screening of various compound libraries can also be used to identify possible drug leads for SAR [46, 47]. Even with these recent discoveries, there are no helicase inhibitors on the market yet. This is can be due to low potency, drug resistance, and cell cytotoxicity. Finding helicase inhibitors is critical due to variability of the virus genome, cost of current treatments, and limited access to impoverished areas where blood borne diseases are more prevalent.

Chapter 2: Methods

Section 2.1: Site Directed Mutagenesis and Protein Expression

pET24a-Hel-2a(JFH) plasmid DNA was extracted and purified using ThermoFisher GeneJet plasmid prep kit from previous work [49]. Plasmid DNA was confirmed on a 1% agarose DNA gel. To create the C292G mutation, mutagenic primers were designed (IDT, Coralville, IA) harboring the desired nucleotide mutation, thymine to guanine as highlighted below.

C292G (+) 5'-CATCATCATATGCGATGAAGGCCACG-3'

C292G (-) 5'-GTAGCATCCACAGCGTGGCCTTCATC-3'

Plasmid DNA was amplified with primers as described by site directed mutagenesis kit QuikChange II XL from Agilent Technologies. After the PCR, products were used to transform into E. coli XL10 cells. Transformed *E. coli* were plated on LB Kanamycin and selected after incubation. Successfully transformed colonies' plasmid DNA were extracted and purified using GeneJet kit (ThermoFisher) following the manufacturer's instructions. Selected plasmids were sequenced (Genewiz, South Plainfield, NJ) before expression and protein purification. Plasmids harboring the desired point mutation were used to transform BL21(DE3) cells as described by Hanson et al. [50]. The new plasmid was named pET24a-Hel-2a(JFH)C292G for storage. Expression and purification yielded about 5 mg of helicase from 2 liters of culture. This is lower than described by Lam *et al.*, [49] possibly due to transformation inefficiency with the cells used at the time and shortened time of culture incubation. Wildtype genotype 2a (JFH1 stain) NS3 helicase was expressed and purified as described above and yielded about 10 mg of helicase from 2 liters of culture, in line with what was reported before.

Section 2.2: Colorimetric ATP Hydrolysis Assays

Initial characterization of the two enzymes was done using a colorimetric ATPase assay, with rates determined from measurements are taken at defined time points. The endpoint assay utilized malachite green, which is sensitive up to 300 µM inorganic phosphate. 30 µL reactions were set up in 96 well clear UV plates as reported by Ndjomou et al. [51]: 25 mM MOPS, pH 6.5, 1.25 mM $MgCl_2$, 5 µg/ml BSA, 0.01% (v/v) Tween20, 150 µM Poly-U RNA, 0–100 nM NS3h, and 1 mM ATP. All components except ATP were mixed. Reactions were initiated with ATP and terminated upon addition of the malachite green solution after 15 minutes at 25^{o}C. ATPase assays were also performed in the absence of RNA following the conditions above, initiated with 100 µM ATP, and utilized the coloring agent BioMol Green (Enzo Life Sciences).

Section 2.3: Continuous coupled ATP Hydrolysis Assay

To confirm the activity seen in the endpoint ATPase assay above, a continuous ATP hydrolysis assay was used in which phosphate production was coupled the action of purine nucleoside phosphorylase [52]. Conditions were: 20 mM pH 7.6 Tris, 1mM $MgCl_2$, 150 µM Poly-U RNA, 200 µM ATP, 100µM 2-amino-6-mercapto-7-methylpurine (Invitrogen), 2.5U/mL Purine nucleoside phosphorylase (Sigma Aldrich), and varying concentrations of NS3h to initiate the assay. Absorbance change was converted to nM phosphate released/second following the protocol described by Webb [52].

Section 2.4: DNA Binding Assay

The DNA binding assay is a fluorescence experiment designed to monitor the anisotropic effect of NS3h binding to Cyanine 5 tagged oligonucleotide as described [53]. Conditions were:

25mM Mops pH 6.5, 1.25mM $MgCl_2$, 5nM Cy5'-dT15, and varying concentrations of NS3h. Fluorescence anisotropy measurements were obtained on a TECAN M1000 PRO at 25°C.

Section 2.5: Helicase Unwinding Assay

A Molecular Beacon-based Helicase Assay (MBHA) was used to monitor the ability of HCV helicase to unwind a DNA substrate. The method was followed as described previously [54]. Assays were performed in a cuvette or a microplate utilizing a Varian Cary Eclipse, or Varioskan Plate reader to collect data. Assay final conditions after addition of 10 mM ATP were as follows: 25 mM MOPS, pH 6.5, 1.25 mM $MgCl_2$, 0.01% Tween20, 5 µg/mL BSA, 10 nM MBHA substrate, 1 mM ATP, and varying concentrations of NS3h. ATP was used to initiate the assay.

Section 2.6: Intrinsic Protein Fluorescence

Intrinsic protein fluorescence can be monitored by observing fluorescence emission at 340 nanometers, while exciting a protein solution at 280 nanometers. First, enzyme concentration was confirmed by absorbance. 100 nM enzyme was used for the assay. Next, the extinction coefficient was calculated for the compound by taking absorbance reading at A_{280} and A_{340}. This was done to further correct for inner filter effects $F_{corr}=F_{obs}*10^{((A_{ex}+A_{em})/2)}$. Next, the drug compound was titrated into a reaction mixture (25 mM MOPS, pH 6.5, 1.25 mM $MgCl_2$, 0.01% Tween20) that does not contain enzyme. This was done to account for either a fluorescent compound or an absorbent compound at the respective wavelengths. This generates a baseline fluorescence/absorbance profile for the compound. Last, the drug compound was titrated into the same reaction mixture, containing 100 nM helicase and fluorescence is observed over a range of inhibitor concentration. Data was corrected for volume dilution effect, inner filter effect, and compound fluorescence. Resulting data was then

corrected data which is plotted against total inhibitor concentration. Data was fit to a one-site binding equation $Y = B_{max}*X/(K_d + X)$ or the quadratic equation (see Fig. 2, legend) to calculate the dissociation constant, K_d.

Chapter 3: Screening for DAAs targeting HCV helicase

Five distinct classes of newly synthesized drug compounds were screened using methods from sections 2.2, 2.4, and 2.5. The following chapter contains data excerpts from the following works:

- Marcella Bassetto, Pieter Leyssen, Johan Neyts, **Mark M. Yerukhimovich,** David N. Frick, and Andrea Brancale. "Shape-based Virtual Screening, Synthesis and Evaluation of Novel Pyrrolone Derivatives as Antiviral Agents against HCV." Bioorganic & Medicinal Chemistry Letters 27.4 (2017): 936-40.
- Marcella Bassetto, Pieter Leyssen, Johan Neyts, **Mark M. Yerukhimovich,** David N. Frick, Matthew Courtney-Smith, and Andrea Brancale. "In Silico Identification, Design and Synthesis of Novel Piperazine-based Antiviral Agents Targeting the Hepatitis C Virus Helicase." European Journal of Medicinal Chemistry 125 (2017): 1115-131.
- Marcella Bassetto, Salvatore Ferla, Pieter Leyssen, Johan Neyts, **Mark M Yerukhimovich,** David N Frick, Rachel O'Donnell, and Andrea Brancale. "Novel Symmetrical Phenylenediamines as Potential Anti-Hepatitis C Virus Agents." Antiviral Chemistry & Chemotherapy (2016): Antiviral Chemistry & Chemotherapy, 04 November 2016.
- Marcella Bassetto, Pieter Leyssen, Johan Neyts, **Mark M. Yerukhimovich,** David N. Frick, and Andrea Brancale. "Computer-aided Identification, Synthesis and Evaluation of Substituted Thienopyrimidines as Novel Inhibitors of HCV Replication." European Journal of Medicinal Chemistry 123 (2016): 31-47.
- Neerja Kaushik-Basu, Nina K. Ratmanova, Dinesh Manvar, Dmitry S. Belov, Ozge Cevik, Amartya Basu, **Mark M. Yerukhimovich**, Evgeny R. Lukyanenko, Ivan A. Andreev, Grigory M. Belov, Giuseppe Manfroni, Violetta Cecchetti, David N. Frick, Alexander V. Kurkin, Andrea, Altieri, and Maria Letizia Barreca. "Bicyclic Octahydrocyclohepta[b]pyrrol-4(1H) one Derivatives as Novel Selective Anti-Hepatitis C Virus Agents." European Journal of Medicinal Chemistry 122 (2016): 319-25.

Section 3.1: Novel Pyrrolone Inhibitors

A ligand-based approach was applied to screen in silico a library of commercially available compounds, with the aim to find novel inhibitors of the HCV replication starting from the study of the viral NS3 helicase. Six structures were selected for evaluation in the HCV sub genomic replicon assay and one hit was found to inhibit the HCV replicon replication in the low

micromolar range. A small series of new pyrrolone compounds was designed and synthesized, and novel structures were identified with improved antiviral activity (Fig. 1, Table I).

Section 3.2: Novel Piperazine Inhibitors

A structure-based virtual screening of commercial compounds was carried out on the HCV NS3 helicase structure, with the aim to identify novel inhibitors of HCV replication. Among a selection of 13 commercial structures, one compound was found to inhibit the sub genomic HCV replicon in the low micromolar range. Different series of new piperazine-based analogues were designed and synthesized, and among them, several novel structures exhibited antiviral activity in the HCV replicon assay. Some of the new compounds were also found to inhibit HCV NS3 helicase function in vitro, and one directly bound NS3 with a dissociation constant of 570 ± 270 nM (Figure 2, Table II).

Section 3.3: Novel Thieno-pyrimidine Inhibitors

A structure-based virtual screening technique was applied to the study of the HCV NS3 helicase, with the aim to find novel inhibitors of the HCV replication. A library of ~450,000 commercially available compounds was analyzed in silico and 21 structures were selected for biological evaluation in the HCV replicon assay. One hit characterized by a substituted thieno-pyrimidine scaffold was found to inhibit the viral replication with an EC50 value in the sub-micromolar range and a good selectivity index. Different series of novel thieno-pyrimidine derivatives were designed and synthesized; several new structures showed antiviral activity in the low or sub-micromolar range (Fig. 3, Table III and IV).

Section 3.4: Novel symmetrical phenylenediamine Inhibitors

Despite the great progress made in the last 10 years, alternative strategies might help improving definitive treatment options against hepatitis C virus infection. With the aim of identifying novel inhibitors of the hepatitis C virus-1b replication targeting the viral NS3 helicase, the structures of previously reported symmetrical inhibitors of this enzyme were rationally modified, and according to docking-based studies, four novel scaffolds were selected for synthesis and evaluation in the hepatitis C virus-1b sub genomic replicon assay. Among the newly designed compounds, one new structural family was found to inhibit the hepatitis C virus-1b replication in the micromolar range. This scaffold was chosen for further exploration and different novel analogues were synthesized and evaluated. Different new inhibitors of the hepatitis C virus genotype 1b replication were identified. Some of the new compounds show mild inhibition of the NS3 helicase enzyme (Table V).

Section 3.5: Novel Bicyclic octahydrocyclohepta[b]pyrrol-4(1H) one Inhibitors

We report the discovery of the bicyclic octahydrocyclohepta[b]pyrrol-4(1H)-one scaffold as a new chemotype with anti-HCV activity on genotype 1b and 2a sub genomic replicons. The most potent compound 34 displayed EC_{50} values of 1.8 μM and 4.5 μM in genotype 1b and 2a, respectively. Compound 34 moderately inhibits helicase unwinding with an IC_{50} of 300 μM and binds helicase with a K_d of 1.1 μM (Fig. 4, Table VI).

Chapter 4: Role of Cys292 in Coupling RNA binding to Helicase-catalyzed ATP Hydrolysis

Section 4.1: Background

HCV NS3h is a super family 2 helicase composed of 3 domains, Rec A-like domains 1 and 2, and domain 3. The helicase has two important catalytic functions that are linked together: ATP hydrolysis and DNA binding/unwinding. The space between domains 1 and 2 forms the ATP binding site (Fig. 5). The groove between domain 3 and the Rec A like domains, forms the DNA/RNA binding site. NS3h belongs to superfamily 2 helicases and encodes conserved regions. One of those regions is the ATPase site which contains Walker Type A and B motifs [38]. NS3h has a conserved 4 residue active site for ATP hydrolysis; DECH box protein. D, E and H, in the Walker B motif (Fig. 5A), function as a metal binding motif that coordinates with the divalent metal cofactor required to activate a water for nucleophilic attack of the γ-phosphate of ATP. Lysine 210, from the Walker type A motif, additionally coordinates the magnesium ion in the active site. Substitutions of other amino acids in the ATPase site in place of the D290, E291, or H293 in Walker B motif, or K210 in Walker A motif, render a defective helicase. Here, substitutions for the C292 in this motif are examined, and they are compared with similar substitutions made elsewhere in the proteins outside the ATP binding site (Fig. 5B). The DNA binding/unwinding site includes by conserved residues T269, T411, R467, W501, and V432 that are all critical to helicase function [39]. The cleft between domains 1 and 2 opens and closes upon ATP binding and hydrolysis causing the protein to move on DNA like an inchworm (Fig. 6).

ATP and RNA (or DNA) can bind independently to HCV helicase, but only when both are bound together will the helicase rapidly hydrolyzed ATP to fuel its motions on RNA (k_{fast}, Fig. 7).

The experiments in this chapter were designed to test how Cys292 coordinate helicase action by measure K_d, K_m, K_m*, K_{RNA}, k_{fast} and k_{slow} for HCV helicase isolated from two different genotypes (1b and 2a) and compare the values with those obtained using helicases in which Cys292 is replaced with a Gly (C292G).

Section 4.2: Results

Site directed mutagenesis was used to generate a plasmid encoding genotype 2a HCV helicase harboring a C292G substitution, and its sequence confirmed by DNA sequencing (Fig, 8).

Unwinding assays reveal very different activity for the two enzymes (Fig. 9). At low concentrations of enzyme, C292G has a significantly lower unwinding rate than wild type. This difference in unwinding rates might be due to the mutant enzyme unwinding fewer base pairs per binding event. The C292G unwinding velocity reaches steady state at high (>500nM) helicase concentration supporting the idea the mutant is less processive than wild type; wild type reaches V_{max} at about 100 nM. It can be seen from Fig. 9 that above 100 nM, wild type helicase, the velocity begins to decline, whereas with the C292G protein rates continues to increase in velocity. This may be due to aggregation of wildtype and steric hindrance as more helicase molecules crowd on the MBHA substrate. The short lag phase for the mutant, seen in Fig. 9, below 100 nM may suggest a few mechanisms. It is possible that the mutant is constantly in the open conformation and thus it takes longer to go through energetic motions to effectively hydrolyze ATP and unwind the substrate. This may not hold true, if the DNA binding isotherms are similar and thermodynamically the same between wild type and mutant. Another possibility is that the mutant binds the MBHA substrate and the open ATPase site is too mobile

and therefore cannot achieve optimal active site configuration. At low enzyme concentration, this might explain the slower rates. At higher concentrations, the fluorescence is a collective measurement of all the substrate being unwound thus no lag is observed.

To probe why the C292G protein might be different from wildtype, we designed experiments to compare K_d, K_m, K_m*, K_{RNA}, k_{fast} and k_{slow} (Fig. 7) for C292G and the wildtype protein.

In the first set of assays, the dissociation constant describing DNA binding (K_d,) was found to be similar for both enzymes (Fig. 10). Others have shown that HCV helicase binds DNA tightly with a ΔG of about -50 kJ/mol [48]. We calculated ΔG of about -51 kJ/mol which concurs with the value previously reported. Both the wild type and C292G mutant bind DNA with similar affinity (Fig. 10). The dissociation constant describing the interaction of RNA in the presence of ATP was probed by determining the amount of RNA needed to stimulated helicase catalyzed ATP hydrolysis by 50% K_{RNA}. The K_{RNA} was about 50% lower for the C292G protein than the wildtype, suggesting a slightly tighter interaction in the presence of ATP (Fig 11).

Both C292G and wildtype have the same ATP hydrolysis rate in the presence of Poly U RNA (Figs. 12, 13). When bound to RNA, the two enzymes have similar turnover rates (Fig. 11), and the observed K_m for ATP is similar for both proteins (Fig. 12).

In contrast, the wildtype and C292G enzymes behave dramatically different in the absence of RNA (Figs. 14, 15). When the enzyme is not bound to RNA, the C292G substitution yields a helicase that can hydrolyze ATP 15 times faster than wildtype in the absence of Poly U RNA (Fig. 14), and the Km for ATP is almost 10 times higher in reactions catalyzed by C292G (Fig. 15), suggesting that ATP binds C292G weaker than wildtype.

Combined, these data also show that the wildtype is stimulated over 20-fold in the presence of nucleic acid, but the C292G protein is only stimulated 1.5-fold. The hypothesis of a mobile ATPase site is supported by the higher K_m value for the C292G, where enzyme concentration is 10 nM and the K_m for ATP is about 10 times higher than the wildtype. Figure 12 confirms that ATP hydrolysis affinity for ATP is similar in the presence of RNA for both enzymes.

Section 4.3: Conclusions

The data presented within gives insight as to the importance of the Cys292 residue. The absence of the cysteine residue may confer an open conformation of the ATPase site that allows for hydrolysis to occur in the absence of nucleic acid. With the more open ATPase site, it may take longer for proper contact to be made for rapid unwinding. ATP binding weakens the helicase-DNA affinity and thus results in a weakly bound state. In this weakly bound state, the helicase can translocate along nucleic acid. Rapid ATP hydrolysis and release of phosphate returns the helicase to a tightly bound conformation with respect to the DNA [55]. The repetition of this cycle causes helicase translocation from 3' to 5'. The similar affinity for DNA shows that the C292G helicase is functional. The activity is further supported by the stimulated ATPase results, showing specific activities are similar for both enzymes. The unstimulated ATPase data show that the mutant can hydrolyze ATP without RNA substrate. That may mean there are more enzymatic motions throughout that break the link of ATP hydrolysis to helicase translocation. That result, coupled with the very different behaviors seen in the unwinding data, may show that the cysteine is necessary to link ATP hydrolysis and helicase unwinding.

In unwinding assay (Fig. 9), at above 100 nM wild type helicase the velocity begins to decline whereas unwinding catalyzed by C292G continues to increase in velocity. This may be

due to aggregation of wildtype and steric hindrance as more helicase molecules crowd on the MBHA substrate. The sigmoidal shape of the curve with the C292G protein (Fig. 9), below 100 nM, may suggest a few mechanisms. It is possible that the mutant is constantly in the open conformation and thus it takes longer to go through energetic motions to effectively hydrolyze ATP and unwind the substrate. This may not hold true, as the DNA binding curves are very similar and thermodynamically the same between wild type and mutant. Another possibility is that the mutant binds the MBHA substrate, and the open ATPase site is too mobile and therefore cannot achieve optimal active site configuration. At low enzyme concentration, this is seen as the lag phase. At higher concentrations, the fluorescence is a collective measurement of all the substrate being unwound.

Since the C292G protein displays the peculiar DNA unwinding characteristic (Fig. 9), it would be interesting to crystalize and using nucleoside analogs, as demonstrated by Gu and Rice [56], to visualize the conformations of apoenzyme, DNA bound, DNA and ATP bound, and DNA and ADP and Pi bound, to understand what step of the enzymatic pathway causes the visible result. The substitution to a glycine would occupy less space in the active site, as well as reduce any electrostatic or steric interaction. From the data presented within, cysteine 292 plays a critical role in linking ATP hydrolysis to DNA unwinding.

TABLES

Compound	EC_{50} (μM)[a,d],[37]	EC_{90} (μM)[b,d]	CC_{50} (μM)[c,d]	SI[e]	Unwinding IC_{50} (μM) [f],[16]
3a (SPECS)	38	149	>204	>4	n.d.
3a (synthesised)	20.3 ± 1.1	61.7 ± 2.7	>205	>10	>1000
3b	4.1 ± 2.5	12.4 ± 6.3	>240	>58	>1000
7a	27.2 ± 7.6	100	112	4	>1000
7b	4.7 ± 0.5	14 ± 4.2	30.3 ± 5.9	6.4	>1000
7c	5.9 ± 1.8	21.6 ± 1.8	97.2 ± 8.7	18	438
7d	4.3 ± 1.5	11.6 ± 0.8	25.7 ± 6.4	6	>1000
7e	16.1 ± 2.7	61.7	156 ± 63.3	9.7	>1000
8a	22.5 ± 0.9	81.1 ± 13.1	>244	>11	>1000
9a	43.1 ± 19.9	–	90.8 ± 26.8	2.1	>1000
(VX-950)	0.8 ± 0.2	–	47	58.8	n.d.
Primuline	–	–	–	–	10 ± 2
Aurintricarboxylic Acid	–	–	–	–	0.3 ± 0.1

Table I: **Pyrrolone compound screening results.** 9 synthesized compounds were screened using an *in vitro* Helicase Unwinding assay, shown in the last column. Compound 7c had moderate inhibition of 438 μM however was cytotoxic above 97 μM.

Compound	EC_{50}(μM)[a,d]	EC_{90}(μM)[b,d]	CC_{50}(μM)[c,d]	SI[e]	Unwinding IC_{50} (μM)[f]
1a	13.8 ± 0.531	–	>182	>13.2	>1000
1b	58.3	–	>104	>1.8	n.d.
1c	19.2	–	>197	>10.3	n.d.
1d	>92.5	>92.5	>92.5	–	n.d.
1e	18.1 ± 1.57	61.1	77.4	4.4	n.d.
1f	82	>166	>166	>2	n.d.
1g	>83.2	>83.2	>83.2	–	n.d.
1h	4.9	–	49.9	10	460 ± 430
1i	76.9 ± 18.2	173	>182	>2.4	n.d.
1l	8.7 ± 5.03	42.9 ± 34.1	97.2 ± 17.1	11.2	310 ± 190
1m	6.5	–	>162	>25	>1000
1n	1.2	–	4.9	3.9	630 ± 270
1o	>172	>172	>172	–	>1000
1p	42.5 ± 15.3	>172	>172	>4	>1000
1q	62 ± 14.4	156	>203	>3.3	n.d.
1r	>207	>207	>207	–	n.d.
1s	56.2 ± 3.2	–	>160	>2.8	>1000
1t	>176	–	>176	–	>1000
1u	39.6 ± 9.03	>182	>182	>4.6	n.d.
8a	>95.9	–	>95.9	–	250 ± 110
8b	>110	–	>110	–	n.d.
8c	>104	>104	>104	–	n.d.
8d	>97.5	>97.5	>97.5	–	n.d.
8e	17.4 ± 5.56	–	>184	>10.6	n.d.
8f	85.8	>87.3	>87.3	>1	n.d.
8g	>87.3	–	>87.3	–	n.d.
8h	10.6	–	>90.5	>8.5	690 ± 350
11a	–	–	>86.6	–	>1000
11d	–	–	>87.9	–	n.d.
11f	>159	>159	>159	–	n.d.
11g	>79.5	–	>79.5	–	n.d.
11h	12 ± 4.24	–	40.8	3.4	n.d.
17	66.7 ± 12.5	164	>173	>2.5	790 ± 270
20	>209	>209	>209	–	n.d.
21	12.1	–	22	1.8	n.d.
23	19.9 ± 6.07	>64	81.5 ± 30.4	4.1	n.d.
24	9.93 ± 3.34	36	48.8 ± 4.8	4.9	n.d.
25	2.21 ± 0.747	4.96	8.77 ± 1.47	4	310 ± 66
26	10.1 ± 0.799	33.5 ± 5.72	63.7 ± 12.8	6.3	n.d.
27	2.12 ± 0.722	–	4.43 ± 0.845	2.1	n.d.
28	3.74 ± 0.878	–	20.5 ± 6.64	5.5	n.d.
29	3.5 ± 0.664	9.44	14.6 ± 1.44	4.2	n.d.
30	6.62 ± 2.34	13.8 ± 6.02	28.7 ± 9.07	4.3	>1000
31	1.3 ± 0.777	3.05 ± 1.12	4.78 ± 1.53	3.7	90 ± 30
32	26.3 ± 6.25	–	138	5.3	n.d.
33	1.98 ± 0.307	–	6.55 ± 1.3	3.3	n.d.
34	4 ± 2.49	–	14 ± 3.4	3.5	>1000
35	12.1 ± 1.36	–	70.8 ± 13	5.8	n.d.
36a	6.59 ± 2.03	–	32.3 ± 7.34	4.9	n.d.
36b	69.2 ± 21	212	>214	>3.1	n.d.
36l	1.7 ± 0.17	–	5.21 ± 1.51	3.1	170 ± 30
37a	9.32 ± 5.44	25.9 ± 6.32	69.1	7.4	>1000
37b	>202	>202	>202	–	n.d.
37c	64.3 ± 2.24	173	>191	>3	n.d.
37l	3.84 ± 1.34	–	20.8 ± 10.7	5.4	>1000
37n	3.03 ± 0.226	–	66.9 ± 50.2	22.1	>1000
39	61.9	–	145	2.3	n.d.
(VX-950)	0.8 ± 0.2	–	47	58.8	n.d.
Primuline	–	–	–	–	10 ± 2
Aurintricarboxylic Acid	–	–	–	–	0.3 ± 0.1

Table II: **Piperazine compound screening results.** 58 synthesized compounds were screened using an *in vitro* Helicase Unwinding assay, shown in the last column. Compound 31 had the best inhibition of the compounds and was selected for further *in vitro* analysis.

Compound	$IC_{50}(\mu M)$			
	Unwinding	ATPase (w RNA)[a]	ATPase (no RNA)[a]	DNA binding[a]
11a	>1000	780 ± 50	760 ± 40	>1000
31a	224	n.d	n.d.	n.d.
37	>1000	>1000	n.d.	675 ± 240
26b	250	333	>1000	>1000
1f	229	n.d	n.d.	n.d.
11g	>1000	>1000	n.d.	827 ± 220
28g	>1000	>1000	n.d.	949 ± 130
26i	306	n.d	n.d.	n.d.
Primuline	10 ± 2	40 ± 12	>200	46 ± 10
Aurintricarboxylic Acid	0.3 ± 0.1	5.1 ± 2.7	3.3 ± 1.7	2.0 ± 0.9

Table III: **Selected Thieno-pyrimidines for helicase inhibition analysis.** 8 compounds were selected for further *in vitro* testing utilizing ATP hydrolysis assay in the presence and absence of Poly U RNA, and DNA binding inhibition.

Compound	Unwinding (IC_{50})	Compound	Unwinding (IC_{50})
1a	>1000	**26b**	250
9a	>1000	**29b**	>1000
11a	>1000	**32b**	>1000
16a	>1000	**1c**	>1000
19a	>1000	**28c**	>1000
20a	>1000	**1d**	>1000
21a	>1000	**1f**	229
25a	>1000	**11f**	>1000
26a	>1000	**28f**	>1000
28a	>1000	**29f**	>1000
29a	>1000	**1g**	>1000
31a	224	**11g**	>1000
32a	>1000	**20g**	>1000
33a	>1000	**25g**	>1000
37	>1000	**28g**	>1000
38	>1000	**16h**	>1000
40	>1000	**26h**	>1000
11b	>1000	**16i**	>1000
17b	>1000	**26i**	306
20b	>1000	**29i**	>1000
25b	>1000		

Table IV: **Thieno-pyrimidine Helicase unwinding assay results.** 41 thieno-pyrimidine derivatives were screened for inhibition of helicase unwinding. Only four compounds yielded measurable inhibition.

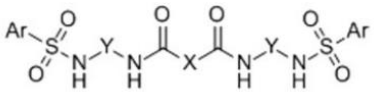

Comp.	Ar	X	Y	EC_{50} (μM)[a,b]	EC_{90} (μM)[b,c]	CC_{50} (μM)[b,d]	SI[e]	Helicase IC_{50} (μM)[d]
[3a]	4-Cl-Ph	*p*-Ph	*p*-Ph	>180	–	>180	–	362
[3b]	4-Me-Ph	*p*-Ph	*p*-Ph	39.9 ± 20.6	>153	>153	>3.8	515
[4a]	4-Cl-Ph	CH=CH	*p*-Ph	>155	>155	>155	–	>1000
[4b]	4-Me-Ph	CH=CH	*p*-Ph	53.1 ± 13.8	>124	>124	>2.3	>1000
[4c]	Ph	CH=CH	*p*-Ph	>173	>173	>173	–	508
[5a]	4-Cl-Ph	$(CH_2)_2$	*p*-Ph	20.4 ± 12	141	>154	>7.5	>1000
[5b]	4-Me-Ph	$(CH_2)_2$	*p*-Ph	66.8 ± 37.8	>165	113	1.7	380
[5c]	Ph	$(CH_2)_2$	*p*-Ph	34.3 ± 3.9	>130	>173	>5	>1000
[5d]	4-*t*Bu-Ph	$(CH_2)_2$	*p*-Ph	12.8 ± 3.3	24.1 ± 14.1	>145	>11.3	n.d.
[5e]	4-CF_3-Ph	$(CH_2)_2$	*p*-Ph	54 ± 46	121	>140	>2.6	>1000
[5f]	4-Biphenyl	$(CH_2)_2$	*p*-Ph	13.3 ± 1.6	63.7 ± 12.1	>137	>10.3	>1000
[5g]	1-Naphthyl	$(CH_2)_2$	*p*-Ph	33.6 ± 7.9	>147	>147	>4.4	>1000
[5h]	8-Quinoline	$(CH_2)_2$	*p*-Ph	>147	>147	>147	–	>1000
[6]	4-Cl-Ph	$(CH_2)_2$	$(CH_2)_2$	>181	>181	>181	–	>1000
(VX-950)	–	–	–	0.8 ± 0.2	–	47	58.8	–
Primuline	–	–	–	–	–	–	–	10 ± 2
Aurintricarboxylic acid	–	–	–	–	–	–	–	0.3 ± 0.1

Table V: **Phenylenediamine derivatives and HCV genotype 1b inhibition.** A series of 14 compounds were screened for helicase unwinding inhibition. 4 compounds had moderate unwinding inhibition, as seen in the last column.

Cpd	CC_{50}[a] (μM)	Huh7/Rep-Feo1b			Huh7.5-FGR-JC1-Rluc2A		
		Inhibition[b] (%)	EC_{50}[c] (μM)	SI[d]	Inhibition[b] (%)	EC_{50}[c] (μM)	SI[d]
6	>200	89 ± 2	7.1 ± 0.73	>28.2	84 ± 2	6.1 ± 0.6	>32.8
22	>200	14 ± 5	ND	ND	42 ± 4	ND	ND
23	>200	41 ± 6	ND	ND	33 ± 11	ND	ND
24	>200	50 ± 4	49.1 ± 3.9	4.1	76 ± 7	14.2 ± 1.5	14.1
25	>200	51 ± 9	59.4 ± 4.8	3.4	91 ± 8	8.7 ± 0.8	22.9
26	>200	NI	ND	ND	38 ± 8	ND	ND
27	>200	15 ± 4	ND	ND	39 ± 11	ND	ND
28	>200	19 ± 4	ND	ND	12 ± 9	ND	ND
29	153 ± 2.2	66 ± 10	28.1 ± 1.1	5.4	48 ± 6	ND	ND
30	>200	32 ± 8	ND	ND	60 ± 1	23.8 ± 1.8	8.4
31	>200	49 ± 5	34.4 ± 1.9	>5.8	94 ± 4	13.0 ± 0.9	>15.4
32	>200	NI	ND	ND	17 ± 7	ND	ND
33	>200	59 ± 1	14.9 ± 1.6	>13.4	95 ± 2	14.3 ± 1.6	>13.9
34	>200	88 ± 1	1.8 ± 0.1	112.4	70 ± 7	4.5 ± 0.8	44.2
35	>200	66 ± 6	14.3 ± 2.5	14.0	58 ± 4	11.6 ± 0.9	17.3
36	>200	63 ± 8	25.3 ± 1.6	7.9	66 ± 5	15.3 ± 2.1	13.1
37	>200	NI	ND	ND	30 ± 10	ND	ND
38	>200	22 ± 2	ND	ND	77 ± 5	27.6 ± 3.6	7.3
39	>200	60 ± 2	27.2 ± 1.6	7.3	73 ± 9	25.8 ± 0.9	7.7
44	>200	25 ± 6	ND	ND	81 ± 7	26.3 ± 3.9	>7.6

Table VI: **Octahydrocyclohepta[b]pyrrol-4(1H) one derivatives and cell based inhibition.** Table shows the cell based inhibition screening in HCV genotypes 1b and 2a. Helicase unwinding data not shown. Compound 34 has the most potent *in vivo* inhibition of HCV replicon.

FIGURES

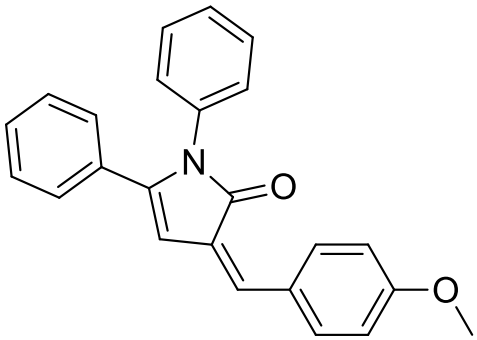

Figure 1: **Structure of synthesized novel pyrrolone HCV NS3h inhibitor 7c.** HCV unwinding assay was performed to characterize the inhibition of 7c on HCV helicase. Compound had moderate IC_{50} of 438 μM.

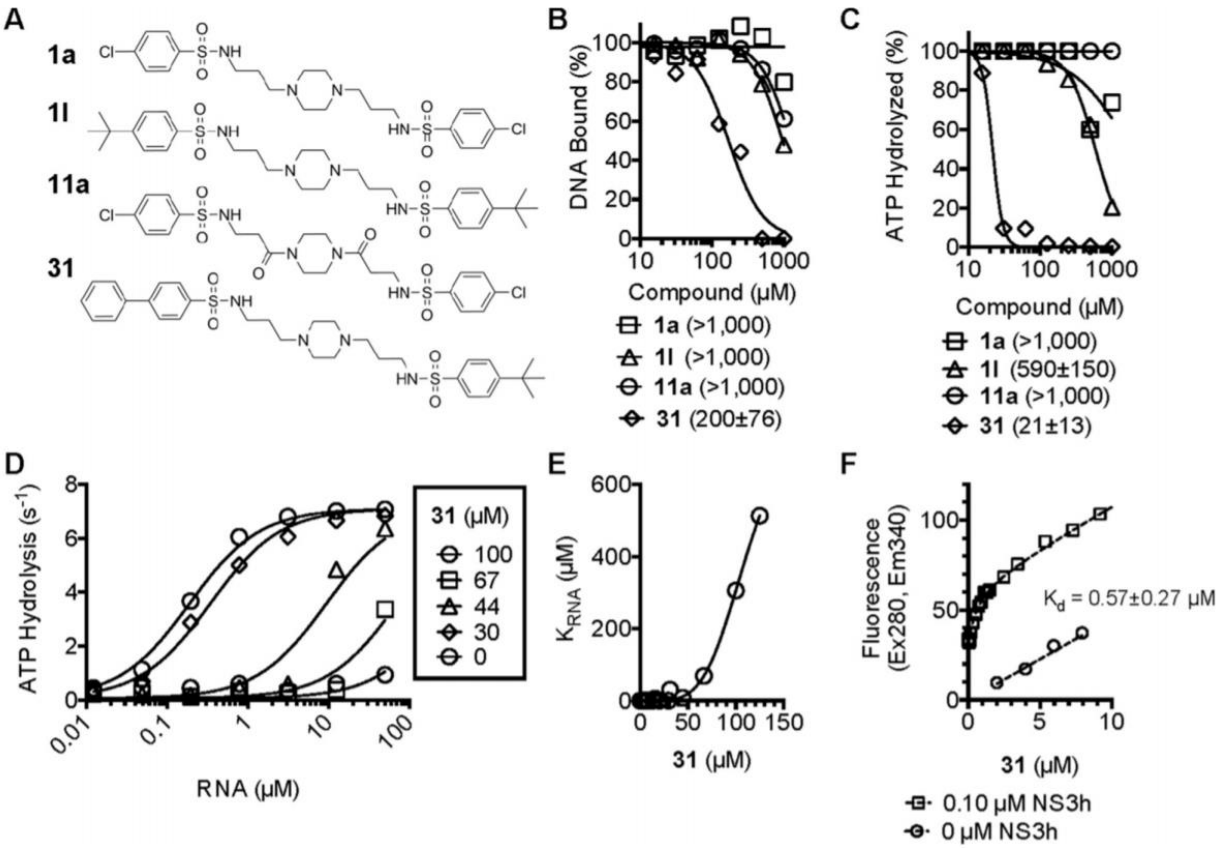

Figure 2: **Piperazine compounds and relevant *in vitro* screening results.** (a) Structures of novel synthesized symmetrical and non-symmetrical piperazine inhibitors. (b) DNA binding assay monitoring percent of displaced ssDNA as a function of inhibitor concentration. Data fit to IC_{50} inhibition equation and numbers list represent 95% confidence intervals of the nonlinear regression. (c) Ability of each compound to inhibit NS3 helicase-catalysed ATP hydrolysis. Numbers in parenthesis are as in (b). (d) Rates of ATP hydrolysis (nM ATP cleaved/s/nM NS3h) observed in the presence of various concentrations of poly(U) RNA and 31. Data are globally fit to $V=(V_{max}*R/K_{RNA} + R) + V_b$ assuming 31 does not affect Vmax. (e) Amount of RNA needed to stimulate ATP hydrolysis to 50% maximum (K_{RNA}) observed at various concentrations of 31. (f) Intrinsic Protein Fluorescence observed with various concentrations of 31 in the absence of NS3h (circles) or in the presence of 100 nM NS3h (squares). Data are globally fit to $F=F_e*(E – EL) + F_s*(L – EL) + F_c*(EL)$ where $EL= ((K_d + L + E) - sqrt((K_d + L + E)^2 - 4*(L*E))))/2$ with the noted dissociation constant and an F_e of 308, F_s of 4.5. and F_c of 641. L is the total concentration of compound 31, E is the concentration of NS3h, K_d is the dissociation constant describing complex formation, F_e is coefficient describing free protein fluorescence, F_s is a coefficient describing free compound 31 fluorescence, and F_c is a coefficient describing the fluorescence of the protein-ligand complex.

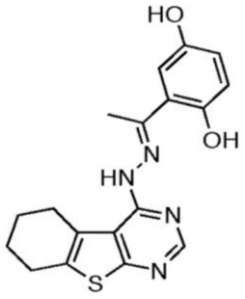

Figure 3: **Structure of Thieno-pyrimidine compound 1a.** Compound did not inhibit the helicase unwinding assay.

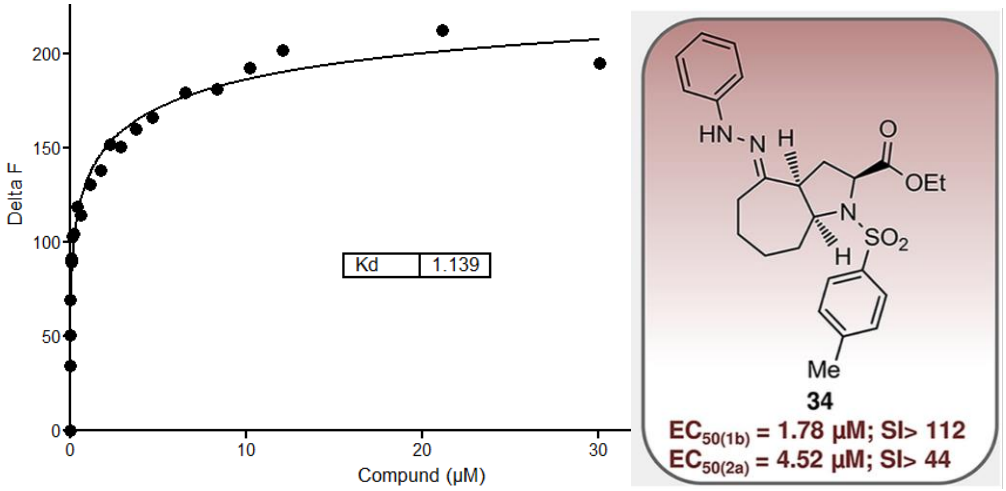

Figure 4: **Intrinsic Protein Fluorescence for Determination of K_d.** Intrinsic Protein Fluorescence observed with various concentrations of 34 in the presence of 100 nM NS3h genotype 1b. Data are fit to the one-site specific binding equation Y = Bmax*X/(Kd + X) to calculate the K_d for specific binding for compound 34. Compound 34 had similar *in vivo* IC_{50} inhibition concentration in genotypes 1b and 2a.

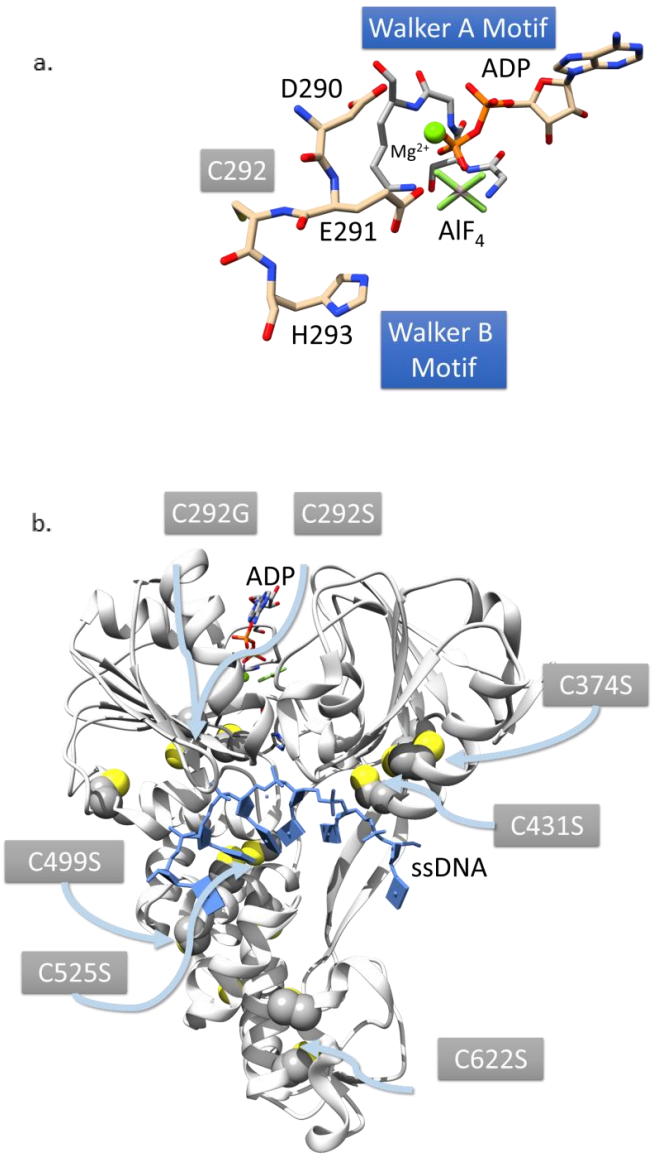

Figure 5: **Positions of Cysteines in of HCV helicase.** Structures were modeled from PDB ID 3KQL showing ATPase site with ADP*AlF_4 and the helicase bound with substrates. (a) Structure of ATPase active site and conserved residues of Walker Type A Motif K210, and Walker type B motif D290, E291, C292, and H293, shown bound with ADP AlF_4 and a magnesium ion. (b) Structure of NS3h bound to ssDNA and ADP*AlF_4 nucleotide analogue. Highlighted Cysteine residues in this study that were mutated are shown in spheres.

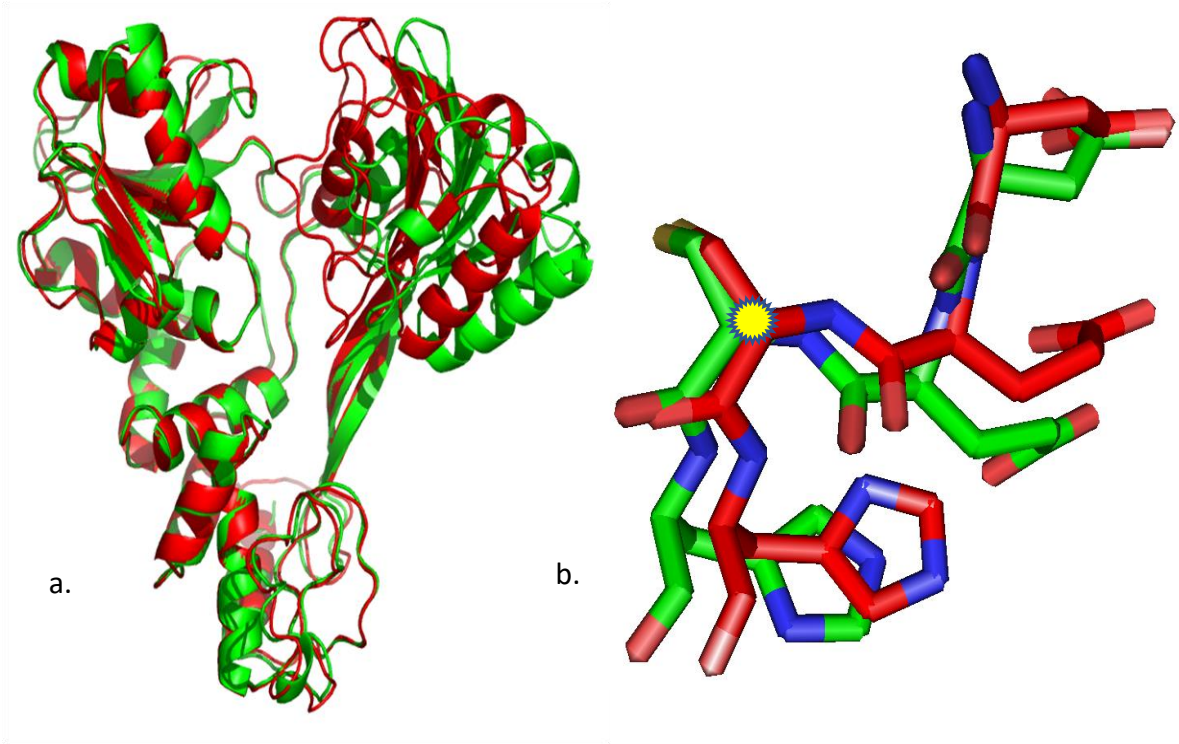

Figure 6: **Structures of open and closed HCV helicase conformations.** (a.) 3KQH (open ATPase site, green) superimposed on 3KQN (closed ATPase site, red) showing the motions of the overall enzyme and (b.) the motions within the ATPase site. Mainly Domain 2 rotates around 1 and 3 upon binding of DNA and ATP. The cysteine is noted by a yellow star in (b) and does not move much relative to the other residues suggesting it may have a key role in an electrostatic interaction.

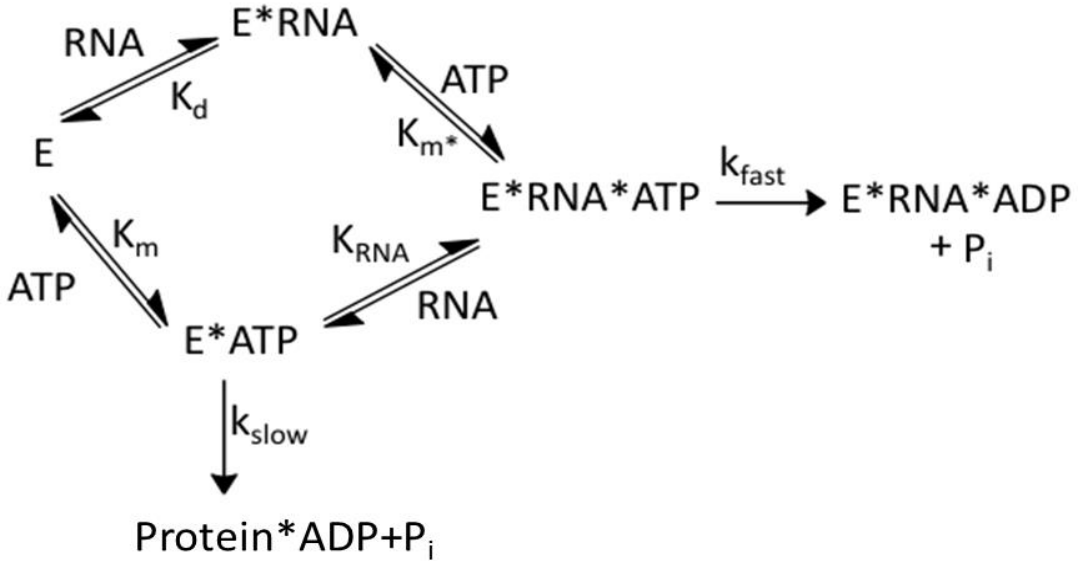

Figure 7: **Random Sequential Mechanism of ATP and RNA binding to HCV helicase.**

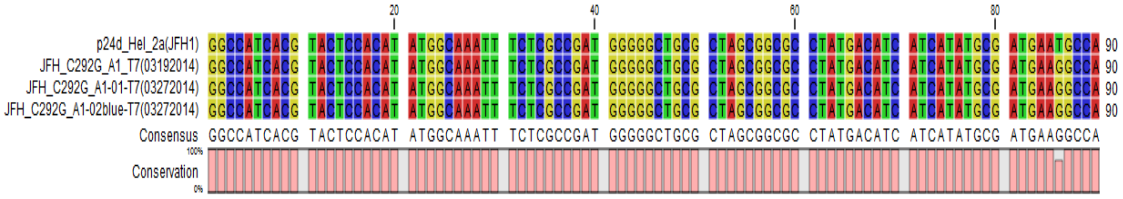

Figure 8: **DNA Sequencing results showing the desired mutation encoding C292G.** After PCR, plasmids were transformed into E. coli. Colonies that grew were selected and the plasmid DNA was extracted and sent for sequencing. Sequencing results were aligned to produce the figure above. The 03192014 plasmid was used to make the recombinant helicase.

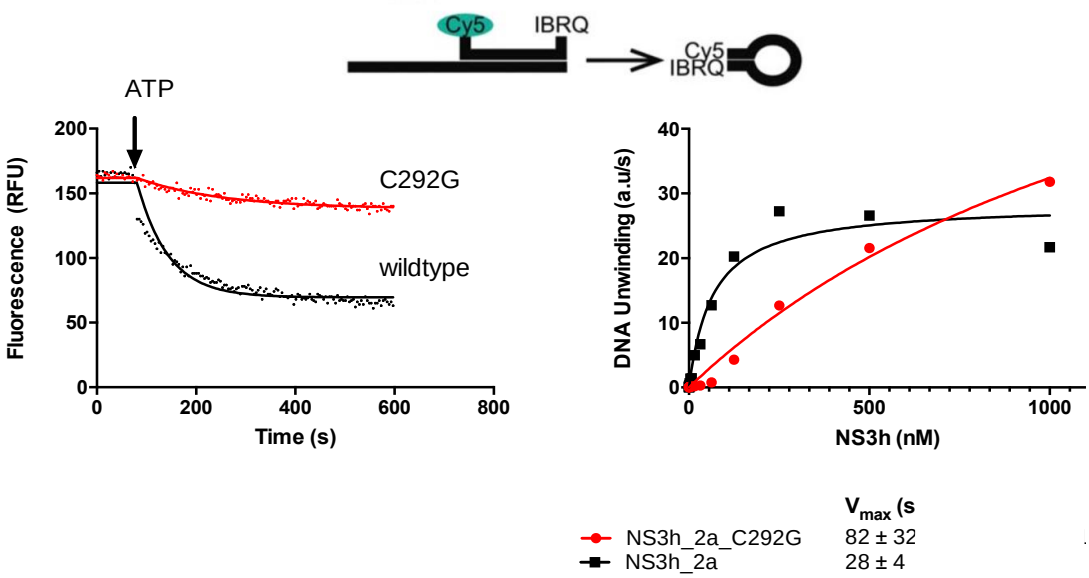

Figure 9: **Helicase unwinding assay with the wildtype and C292G helicases** Molecular beacon helicase assay was used to characterize the unwinding of the mutant C292G versus the wildtype. Various concentrations of both enzymes were used. The raw data (right) was fit to a user defined equation [54]. The fit exported a DNA unwinding rate, a.u./sec, which is the initial velocity time the amplitude. The rates were then fit to Michaelis Menten equation to estimate V_{max}. Two remarkably different enzymes can be seen. It takes about 5 times more of mutant helicase to reach a similar unwinding rate as 50nM wildtype. It is also visible that the mutant may undergo a slower mechanism at lower concentrations as there is a small lag phase up to 100 nM enzyme concentration.

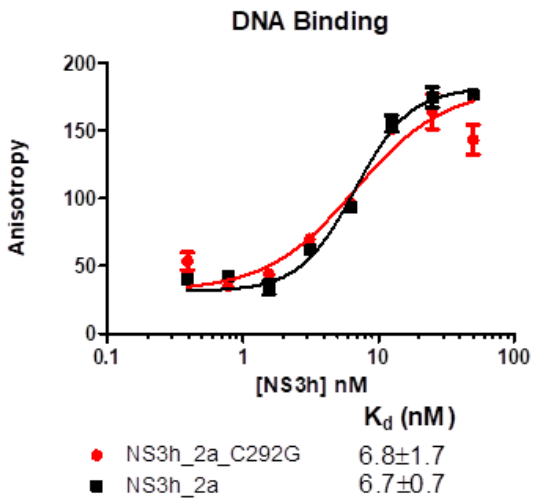

Figure 10: **DNA binding assays to characterize dissociation constant for ssDNA.** Enzyme is titrated into a premix containing 10 nM ssDNA Cy5'-dT15. Fluorescence anisotropy is measured and data is fitted to a one site substrate binding equation Y = Bmax*X/(Kd + X). Genotype 2a wild type and C292G mutant have similar affinity for single stranded DNA confirming the mutation in the ATPase did not affect the nucleic acid binding site.

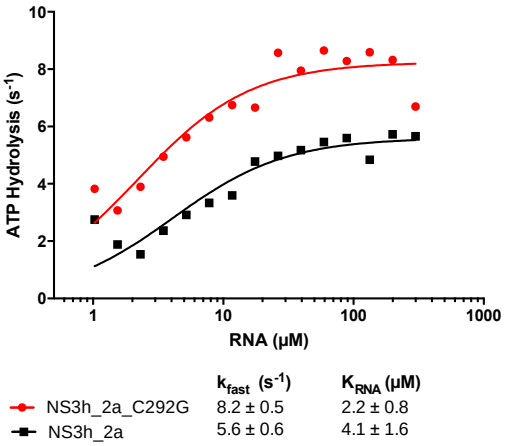

Figure 11: **ATPase assay to approximate enzyme affinity for Poly-U RNA (K_{RNA}).** A stimulated ATPase assay was used to characterize the affinity for RNA. A reaction mixture containing 10nM helicase was pipetted into a 96 well plate. A 16-point dilution of Poly U RNA was added to the wells and the assay was initiated with 10mM ATP. Reaction was run for 900 seconds at which point it was quenched by the coloring reagent. Data was converted to velocity (s^{-1}) and plotted against RNA concentration. Then data was fit with the Michaelis Menten equation, where K_m was used as an approximation for affinity for RNA. The C292G mutant is faster at hydrolyzing ATP and binds RNA slightly tighter than wildtype.

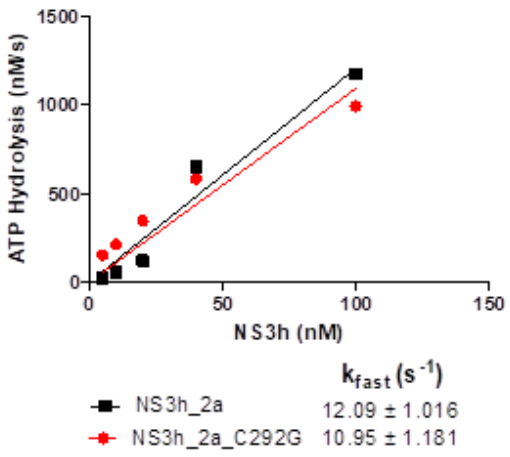

Figure 12: **Stimulated ATPase to characterize specific activity in the presence of RNA.** Enzyme was premixed with Poly-U RNA and the assay was initiated with 10 mM ATP. An endpoint malachite green assay was used quench the reaction after 900 seconds. Absorbance data were converted to nM/sec rates using a known phosphate standard. Rates were plotted and fit with a linear regression to generate the figure above. The single Cys292 mutant behaved similar to the wildtype showing the C292G enzyme is still active.

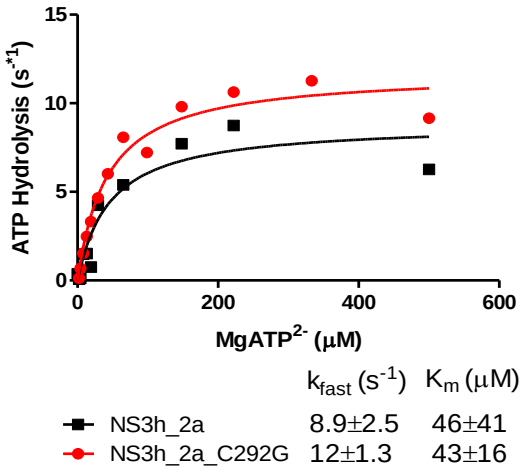

Figure 13: **Stimulated ATPase assay to estimate affinity for Mg*ATP.** Enzyme was premixed with Poly-U RNA and the assay was initiated with 10mM Mg*ATP. An endpoint malachite green assay was used to detect the hydrolysis of ATP over 900 seconds. Results were plotted and fit with a Michaelis Menten equation to estimate the affinity of NS3h to Mg*ATP. Data varied between the genotype 1b enzymes, however, the 2a wildtype and the 2a C292G mutant behaved similarly. This shows both enzymes hydrolyze ATP similarly in the presence of nucleic acid. High concentrations of magnesium are known to inhibit helicase function and may explain the declining rate at the highest concentration point.

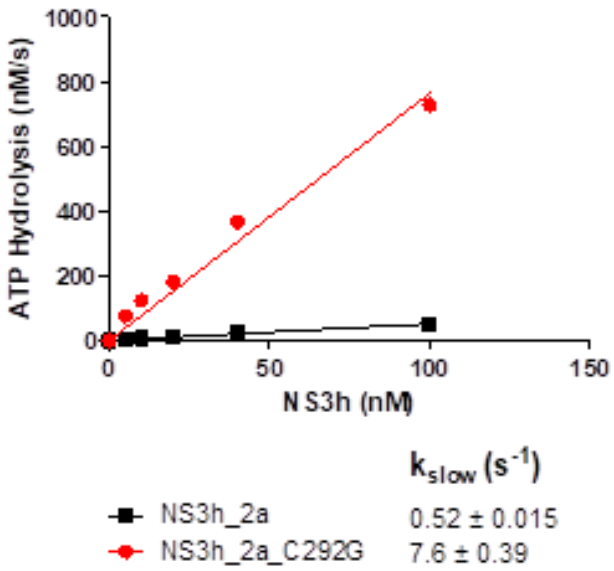

Figure 14: **Unstimulated ATPase to characterize the specific activity of both enzymes**. Enzymatic assay without Poly-U RNA was initiated with 1 mM ATP. A Biomol Green reagent was used to terminate the assay after 900 seconds. Each point is a well on a 96 well plate. Raw absorbance was converted to a rate, nM/sec, using a known phosphate standard. Rates were then plotted and fit with a linear regression to yield a slope k_{slow}. Notice the Cysteine 292 containing mutant has about a 15 times faster ATP hydrolysis rate.

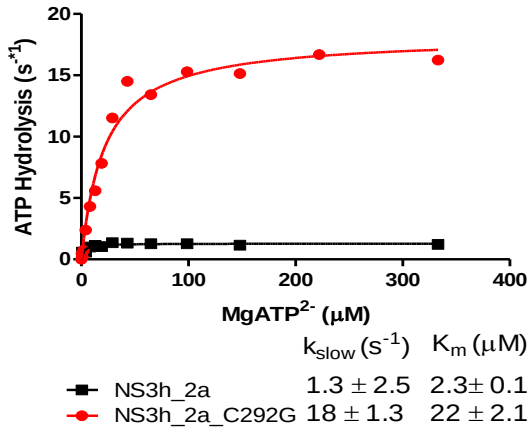

Figure 15: **Unstimulated ATPase assay to estimate affinity for ATP.** Enzymatic assay without Poly-U RNA was initiated with 1 mM Mg*ATP. A Biomol Green reagent was used to terminate the assay after 900 seconds. Results were plotted and fit with Michaelis Menten to estimate affinity for Mg*ATP. Notice the Cysteine 292 containing mutants all have higher rates of ATP hydrolysis than wildtype, as well as higher Km for Mg*ATP.

BIBLIOGRAPHY

1. "Hepatitis C." *World Health Organization*. World Health Organization, 1 Oct. 2017. Web. 13 Dec. 2017.

2. "HIV and Viral Hepatitis." *HIV/AIDS*. Centers for Disease Control and Prevention, 1 June 2016. Web. 13 Dec. 2017.

3. Gu, M., et al. "Structures of Hepatitis C Virus Nonstructural Proteins Required for Replicase Assembly and Function." Current Opinion in Virology 3.2 (2013): 129-36. Print.

4. Morikawa, K., et al. “Nonstructural Protein 3-4A: The Swiss Army Knife of Hepatitis C Virus.” Journal of Viral Hepatitis 18.5 (2011): 305–315. Print

5. Lemke, C., et al. "Combined X-ray, NMR, and Kinetic Analyses Reveal Uncommon Binding Characteristics of the Hepatitis C Virus NS3-NS4A Protease Inhibitor BI 201335." The Journal of Biological Chemistry 286.13 (2011): 11434-43. Print.

6. Raney, K., et al. "Hepatitis C Virus Non-structural Protein 3 (HCV NS3): A Multifunctional Antiviral Target." The Journal of Biological Chemistry 285.30 (2010): 22725-31. Print.

7. Landro, J., et al. "Mechanistic Role of an NS4A Peptide Cofactor with the Truncated NS3 Protease of Hepatitis C Virus: Elucidation of the NS4A Stimulatory Effect via Kinetic Analysis and Inhibitor Mapping." Biochemistry 36.31 (1997): 9340-348. Print.

8. Steinkühler, C., et al. "Product Inhibition of the Hepatitis C Virus NS3 Protease." Biochemistry 37.25 (1998): 8899-905. Print.

9. Ingallinella, A., et al. "Potent Peptide Inhibitors of Human Hepatitis C Virus NS3 Protease Are Obtained by Optimizing the Cleavage Products." Biochemistry 37.25 (1998): 8906-914. Print.

10. Llinàs-Brunet, M., et al. "Discovery of a Potent and Selective Noncovalent Linear Inhibitor of the Hepatitis C Virus NS3 Protease (BI 201335)." Journal of Medicinal Chemistry 53.17 (2010): 6466-76. Print.

11. Scola, P., et al. "Discovery and Early Clinical Evaluation of BMS-605339, a Potent and Orally Efficacious Tripeptidic Acylsulfonamide NS3 Protease Inhibitor for the Treatment of Hepatitis C Virus Infection." Journal of Medicinal Chemistry 57.5 (2014): 1708-29. Print.

12. Liverton, N., et al. "Molecular Modeling Based Approach to Potent P2-P4 Macrocyclic Inhibitors of Hepatitis C NS3/4A Protease." Journal of the American Chemical Society 130.14 (2008): 4607-9. Print.

13. Pilot-Matias, T., et al. "In Vitro and In Vivo Antiviral Activity and Resistance Profile of the Hepatitis C Virus NS3/4A Protease Inhibitor ABT-450." Antimicrobial Agents and Chemotherapy 59.2 (2015): 988-97. Print.

14. Harper, S., et al. "Discovery of MK-5172, a Macrocyclic Hepatitis C Virus NS3/4a Protease Inhibitor." ACS Medicinal Chemistry Letters 3.4 (2012): 332-6. Print.

15. O'Meara, J., et al. "Molecular Mechanism by Which a Potent Hepatitis C Virus NS3-NS4A Protease Inhibitor Overcomes Emergence of Resistance." The Journal of Biological Chemistry 288.8 (2013): 5673-81. Print.

16. Luo, G., et al. "De Novo Initiation of RNA Synthesis by the RNA-Dependent RNA Polymerase (NS5B) of Hepatitis C Virus." The Journal of Virology 74.2 (2000): 851-863. Print.

17. Behrens, S., et al. "Identification and Properties of the RNA-dependent RNA Polymerase of Hepatitis C Virus." The EMBO Journal 15.1 (1996): 12-22. Print.

18. Harrus, D., et al. "Further Insights into the Roles of GTP and the C Terminus of the Hepatitis C Virus Polymerase in the Initiation of RNA Synthesis." The Journal of Biological Chemistry 285.43 (2010): 32906-18. Print.

19. Caillet-Saguy, C., et al. "An Objective Assessment of Conformational Variability in Complexes of Hepatitis C Virus Polymerase with Non-Nucleoside Inhibitors." Journal of Molecular Biology 414.3 (2011): 370-84. Print.

20. Sofia, M., et al. "Discovery of a β- D -2′-Deoxy-2′-α-fluoro-2′-β- C -methyluridine Nucleotide Prodrug (PSI-7977) for the Treatment of Hepatitis C Virus." Journal of Medicinal Chemistry 53.19 (2010): 7202-218. Print.

21. Murakami, E., et al. "Mechanism of Activation of PSI-7851 and Its Diastereoisomer PSI-7977." The Journal of Biological Chemistry 285.45 (2010): 34337-47. Print.

22. Lam, A., et al. "Genotype and Subtype Profiling of PSI-7977 as a Nucleotide Inhibitor of Hepatitis C Virus." Antimicrobial Agents and Chemotherapy 56.6 (2012): 3359-3368. Print.

23. Liu, Y., et al. "Identification of Aryl Dihydrouracil Derivatives as Palm Initiation Site Inhibitors of HCV NS5B Polymerase." Bioorganic & Medicinal Chemistry Letters 22.11 (2012): 3747-750. Print.

24. Kati, W., et al. "In Vitro Activity and Resistance Profile of Dasabuvir, a Nonnucleoside Hepatitis C Virus Polymerase Inhibitor." Antimicrobial Agents and Chemotherapy 59.3 (2015): 1505-11. Print.

25. Sevrioukova, I., et al. "Structure and Mechanism of the Complex between Cytochrome P4503A4 and Ritonavir." Proceedings of the National Academy of Sciences 107.43 (2010): 18422. Print.

26. Shirota, Y., et al. "Hepatitis C Virus (HCV) NS5A Binds RNA-dependent RNA Polymerase (RdRP) NS5B and Modulates RNA-dependent RNA Polymerase Activity." Journal of Biological Chemistry 277.13 (2002): 11149-1155. Print.

27. Arima, N., et al. "Modulation of Cell Growth by the Hepatitis C Virus Nonstructural Protein NS5A." Journal of Biological Chemistry 276.16 (2001): 12675-2684. Print.

28. Ghosh, A., et al. "Hepatitis C Virus NS5A Protein Modulates Cell Cycle Regulatory Genes and Promotes Cell Growth." Journal of General Virology 80.5 (1999): 1179-183. Print.

29. Lan, K., et al. "HCV NS5A Interacts with P53 and Inhibits P53-mediated Apoptosis." Oncogene 21.31 (2002): 4801-4811. Print.

30. Macdonald, A. "Hepatitis C Virus NS5A: Tales of a Promiscuous Protein." Journal of General Virology 85.9 (2004): 2485-502. Print.

31. Elazar, M., et al. "Amphipathic Helix-Dependent Localization of NS5A Mediates Hepatitis C Virus RNA Replication." The Journal of Virology 77.10 (2003): 6055-6061. Print.

32. Lemm, J., et al. "Identification of Hepatitis C Virus NS5A Inhibitors." The Journal of Virology 84.1 (2010): 482-91. Print.

33. Ascher, D., et al. "Potent Hepatitis C Inhibitors Bind Directly to NS5A and Reduce Its Affinity for RNA." Scientific Reports 4 (2014): 4765. Print.

34. Guedj, J., et al. "Modeling Shows That the NS5A Inhibitor Daclatasvir Has Two Modes of Action and Yields a Shorter Estimate of the Hepatitis C Virus Half-life." Proceedings of the National Academy of Sciences 110.10 (2013): 3991. Print.

35. Cheng, G., et al. "1191 GS-5816, A SECOND-GENERATION HCV NS5A INHIBITOR WITH POTENT ANTIVIRAL ACTIVITY, BROAD GENOTYPIC COVERAGE AND A HIGH RESISTANCE BARRIER." Journal of Hepatology 58 (2013): S484-485. Print.

36. Lawitz, E., et al. "A Phase 1, Randomized, Dose-ranging Study of GS-5816, a Once-daily NS5A Inhibitor, in Patients with Genotype 1–4 Hepatitis C Virus." Journal of Viral Hepatitis 22.12 (2015): 1011-019. Print.

37. Ryan, B. “The 2017 Hepatitis C Treatment Pipeline.” HepMag, 15 May 2017, Web, 13 December 2017.

38. Kim, J., et al. "Hepatitis C Virus NS3 RNA Helicase Domain with a Bound Oligonucleotide: The Crystal Structure Provides Insights into the Mode of Unwinding." Structure 6.1 (1998): 89-100. Print.

39. Frick, D. “The Hepatitis C Virus Replicase: Insights into RNA-dependent RNA Replication and Prospects for Rational Drug Design.” Current Organic Chemistry 8 (2004): 223-41. Print.

40. Chen, C., et al. "Structure-based Discovery of Triphenylmethane Derivatives as Inhibitors of Hepatitis C Virus Helicase." Journal of Medicinal Chemistry 52.9 (2009): 2716-23. Print.

41. Maga, G., et al. "Specific Targeting of Hepatitis C Virus NS3 RNA Helicase. Discovery of the Potent and Selective Competitive Nucleotide-Mimicking Inhibitor QU663 †." Biochemistry 44.28 (2005): 9637-644. Print.

42. Bassetto, M., et al. "Shape-based Virtual Screening, Synthesis and Evaluation of Novel Pyrrolone Derivatives as Antiviral Agents against HCV." Bioorganic & Medicinal Chemistry Letters 27.4 (2017): 936-40. Print.

43. Bassetto M., et al. "In Silico Identification, Design and Synthesis of Novel Piperazine-based Antiviral Agents Targeting the Hepatitis C Virus Helicase." European Journal of Medicinal Chemistry 125 (2017): 1115-131. Print.

44. Bassetto M., et al. "Computer-aided Identification, Synthesis and Evaluation of Substituted Thienopyrimidines as Novel Inhibitors of HCV Replication." European Journal of Medicinal Chemistry 123 (2016): 31-47. Print.

45. Bassetto M., et al. "Novel Symmetrical Phenylenediamines as Potential Anti-Hepatitis C Virus Agents." Antiviral Chemistry and Chemotherapy 24.5-6 (2015): 155-60. Print.

46. Li, K., et al. "Optimization of Potent Hepatitis C Virus NS3 Helicase Inhibitors Isolated from the Yellow Dyes Thioflavine S and Primuline." Journal of Medicinal Chemistry 55.7 (2012): 3319-30. Print.

47. Andreev, I., et al. "Discovery of the 2-phenyl-4,5,6,7-Tetrahydro-1H-indole as a Novel Anti-Hepatitis C Virus Targeting Scaffold." European Journal of Medicinal Chemistry 96 (2015): 250-58. Print.

48. Levin, M., et al. "Helicase from Hepatitis C Virus, Energetics of DNA Binding." Journal of Biological Chemistry 277.33 (2002): 29377-9385. Print.

49. Lam, A., et al. “Hepatitis C Virus NS3 ATPases/Helicases from Different Genotypes Exhibit Variations in Enzymatic Properties.” Journal of Virology 77.7 (2003): 3950–3961. Print.

50. Hanson, A., et al. “Identification and Analysis of Inhibitors Targeting the Hepatitis C Virus NS3 Helicase.” Methods in enzymology 511 (2012): 463–483. Print.

51. Ndjomou, J., et al. “Fluorescent Primuline Derivatives Inhibit Hepatitis C Virus NS3-Catalyzed RNA Unwinding, Peptide Hydrolysis and Viral Replicase Formation.” Antiviral research 96.2 (2012): 245–255. Print.

52. Webb, M. “A continuous spectrophotometric assay for inorganic phosphate and for measuring phosphate release kinetics in biological systems”. Proceeding of the National Academy of Sciences 89.11 (2011): 4884-4887. Print.

53. Mukherjee, S., et al. “Identification and Analysis of Hepatitis C Virus NS3 Helicase Inhibitors Using Nucleic Acid Binding Assays.” Nucleic Acids Research 40.17 (2012): 8607–8621. Print.

54. Hanson, A., et al. “Identification and Analysis of Inhibitors Targeting the Hepatitis C Virus NS3 Helicase.” Methods in enzymology 511 (2012): 463–483. Print.

55. Levin, M., et al. "A Brownian Motor Mechanism of Translocation and Strand Separation by Hepatitis C Virus Helicase." Nature Structural & Molecular Biology 12.5 (2005): 429-35. Print.

56. Gu, M., et al. "Three Conformational Snapshots of the Hepatitis Virus NS3 Helicase Reveal a Ratchet Translocation Mechanism." Proceedings of the National Academy of Sciences of the United States of America 107.2 (2010): 521-28. Print.